JOURNAL OF MATERIALS SCIENCE 31 (1996) 4017–4023

Characterization of corrosion products formed on a rapidly solidified Mg based EA55RS alloy

Y. LI, J. LIN, F. C. LOH, K. L. TAN
Department of Physics, National University of Singapore, 0511, Singapore
H. JONES
Department of Engineering Materials, Sheffield University, Sheffield, UK

Surface characterization of the corrosion products formed on the surfaces of rapidly solidified Mg based EA55RS (Mg–5 wt% Al–5 wt% Zn–5 wt% Nd) extrusion immersed in a 3% NaCl solution saturated with $Mg(OH)_2$ has been carried out using X-ray photoelectron spectroscopy (XPS), Auger electron spectroscopy (AES), secondary ion mass spectrometry (SIMS), X-ray diffraction (XRD) and scanning electron microscopy (SEM). The surfaces of both pristine and corroded samples have been found to consist mainly of $Mg(OH)_2$ and MgO. XPS and AES results show that Nd and Zn are not present on the surfaces of either pristine or corroded samples and depth profiling using SIMS shows that there is depletion of Nd on the surfaces.

1. Introduction

In general, magnesium alloys produced by conventional ingot metallurgy processing exhibit poor corrosion resistance. The application of rapid solidification (RS) processing can result in the refinement of both matrix grains and intermetallic particles, extension of solid solubility, formation of non-equilibrium phases (including crystalline, quasi-crystalline and non-crystalline) and improved chemical homogeneity. RS processing of appropriate magnesium alloys can improve their corrosion resistance by contributing towards the formation of protective films and elimination of microgalvanic effects. As a result, a number of workers [1–14] have studied the effect of RS processing and alloy elements on the corrosion resistance of Mg based alloys, with the emphasis on Mg–Al based alloys.

A range of magnesium alloys of novel composition has been developed recently by Allied–Signal based on vacuum hot pressing and extrusion or forging of pulverized melt spun materials [1, 2]. Several of these alloys, including EA55RS (Mg–5 Al–5 Zn–5 Nd, wt %), combine exceptional strength with corrosion resistance. It was reported [1, 2] that the corrosion resistance of EA55RS alloy was superior to that of conventionally cast Mg alloys, such as AZ91, and could even approach that of 2041 aluminium alloys [1].

In the present work, the surface characteristics of EA55RS samples have been studied both as-received and after immersion in 3% NaCl solution. These studies have been carried out using X-ray photoelectron spectroscopy (XPS), Auger electron spectroscopy (AES), secondary ion mass spectrometry (SIMS), scanning electron microscopy (SEM) and X-ray diffraction (XRD).

2. Experimental procedure

The samples of EA55RS extrusion were supplied in the as-extruded condition by Magnesium Electron Ltd and British Aerospace. Pieces of dimensions of $10 \times 10 \times 3\ mm^3$ were cut from the extrusion and were ground and polished, finished with 2 μm MgO. A 3% NaCl solution saturated with $Mg(OH)_2$ was used for the corrosion test [3]. These immersion tests were carried out in a glass container containing the solution at $23.0 \pm 0.5\,^{\circ}C$ for periods of immersion between 5 min to 24 h. After immersion, each specimen was carefully washed with water and acetone and finally air dried.

XPS and AES experiments were carried out in a VG ESCALAB MKII spectrometer at a constant analyser pass energy of 20 eV. MgK_α X-rays (1253.6 eV photon, 120 W) were used as the excitation source in XPS, while an electron beam of 5 keV was used in AES. Charging shift in XPS measurements ranged from ~2 to ~5 eV depending on the immersion time, and was corrected using the major C1s peak at binding energy 285.0 eV as a reference. The SIMS experiments were performed in a VG SIMSLAB system. Both the XPS–AES and SIMS chambers were connected via a preparation chamber, the normal operating pressure in all chambers was $< 2 \times 10^{-7}$ Pa during the course of the experiments. The primary ion source of SIMS was a 9 keV, 100 nA Ar^+ beam, which was incident on the sample surface at 45° with a reduced area mode. X-ray diffraction was performed in a Philips 1700

0022–2461

diffractometer with CuK_α radiation and SEM experiments were carried out in a Jeol 50 equipment.

3. Results

3.1. SEM and XRD

Fig. 1 shows the SEM micrographs of an as-polished sample and one after immersion in 3% NaCl for 1 h. Energy dispersive spectroscopy (EDX) analysis (Fig. 2) shows that the oxygen content increases as time of immersion increases. Fig. 3 shows the XRD profile for the sample corroded for 24 h, indicating that only α Mg and $Mg(OH)_2$ and no other phases are present on the sample surface.

3.2. XPS

3.2.1. Results for pristine sample

Fig. 4 is an XPS survey spectrum of the pristine Mg–Al–Zn–Nd sample, indicating the presence of oxygen, carbon, magnesium and aluminium at the surface. Nd and Zn are not evident at the surface. Fig. 5a gives the XPS O1s core-level spectrum of the pristine sample. This shows the O1s peak is located at the binding energy of 531.2 eV, with a tail of low intensity at a higher binding energy around 533.6 eV. According to the known data [15], the main peak at ~531 eV may be assigned to hydroxide oxygen, while those photoelectrons observed at higher binding energies, around 533.6 eV, may be attributed to the absorbed water on the sample surface. The Mg2p core-level spectrum (Fig. 6a) of the pristine sample consists of a strong peak at 49.4 eV and a very weak one at 51.8 eV. Both the metallic Mg and the Mg hydroxide have been reported [15] to have the same binding energy at 49.5 eV, and they may both contribute to the intensity of this peak. The weak one at 51.8 eV may arise from Mg oxide on the surface [15]. Fig. 7a is the Al2p core-level spectrum of the pristine sample. It is broad and may be composed of two component peaks at 72.8 and 74.6 eV according to the peak synthesis results. On the basis of known data

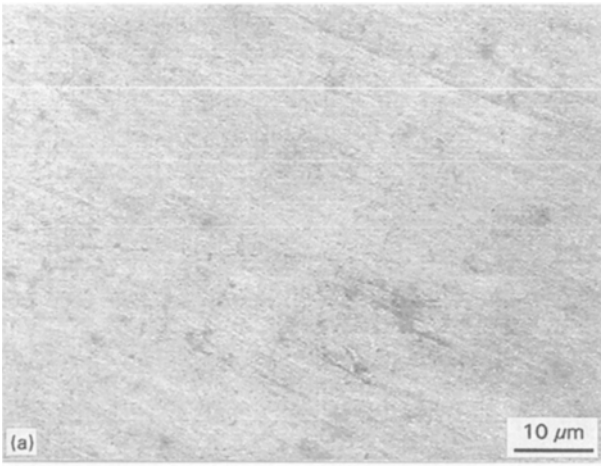

Figure 1 SEM micrographs showing (a) pristine surface of EA55RS, and (b) surface after immersion in 3% NaCl solution for 1 h.

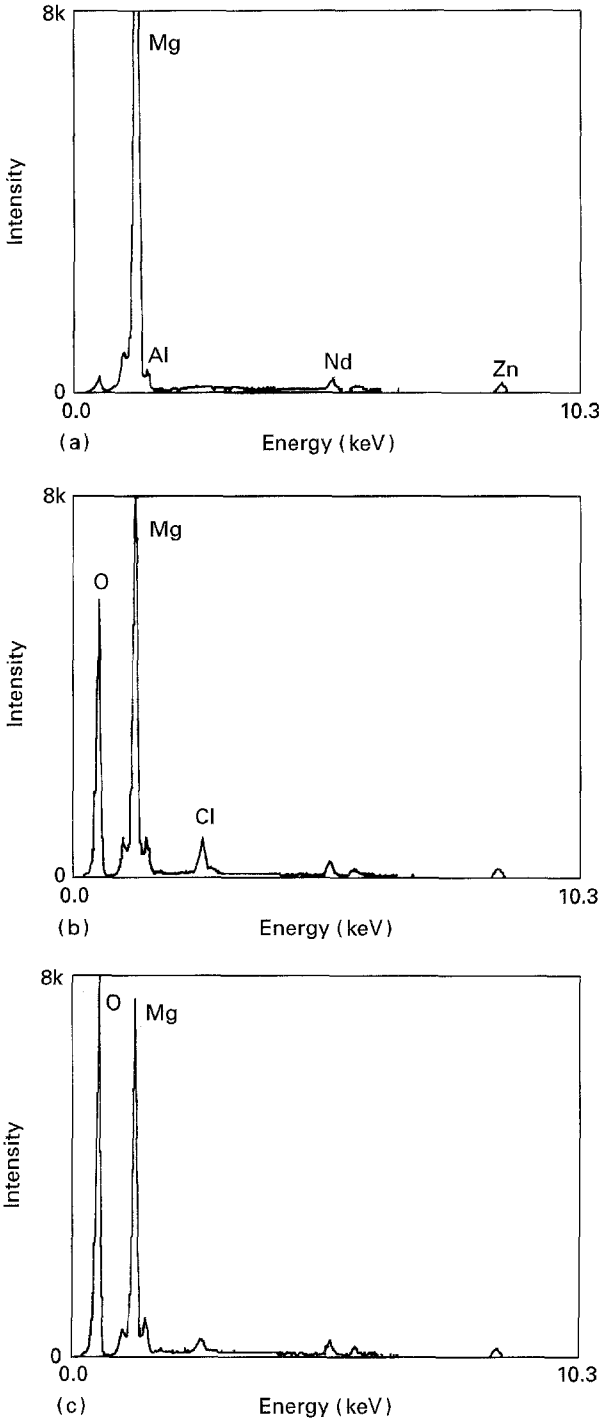

Figure 2 Montage of windowless EDX analysis of EA55RS after immersion in 3% NaCl solution for different lengths of time: (a) pristine sample, (b) after 20 min, and (c) after 1 h.

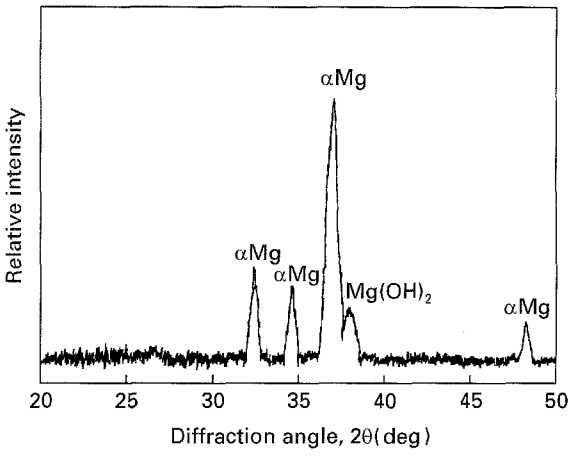

Figure 3 XRD result for EA55RS after immersion in 3% NaCl solution for 24 h showing only αMg and $Mg(OH)_2$ present on the sample surface.

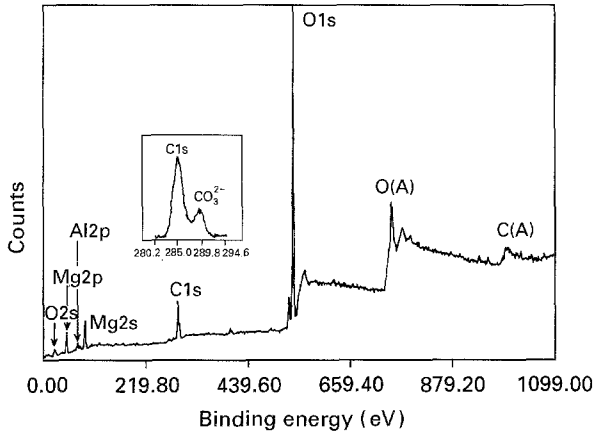

Figure 4 XPS wide-scan spectrum of EA55RS pristine sample. The C1s core-level spectrum is also included.

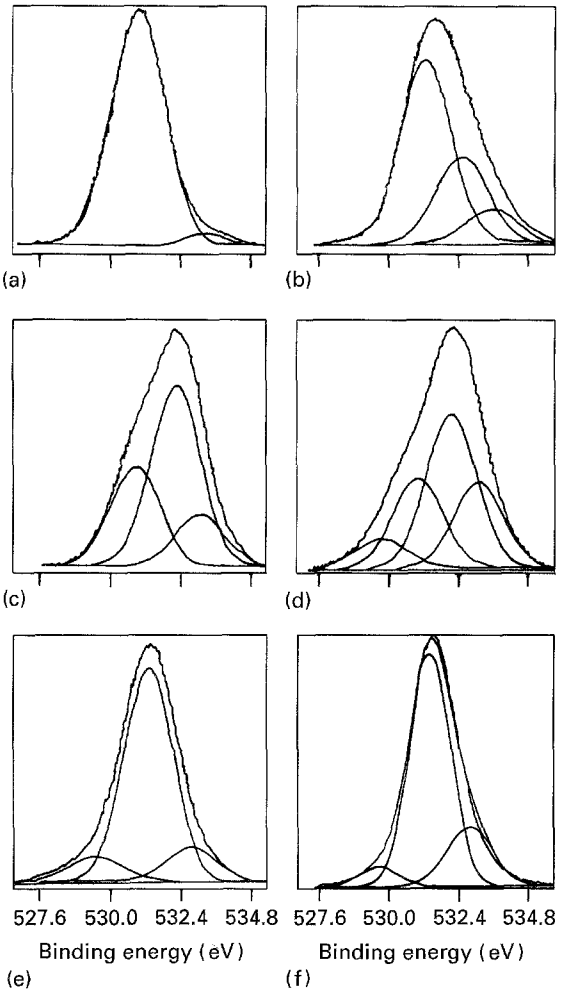

Figure 5 XPS O1s core-level spectra of EA55RS sample after immersion in 3% NaCl solution for different lengths of time: (a) pristine sample, (b) after 15 min, (c) after 20 min, (d) after 30 min, (e) after 1 h, and (f) same as (e), but the take-off angle of photoelectrons with respect to the sample surface is 20°.

[15] the peak at 72.8 eV is assigned to metallic Al, while the one at 74.6 eV is assigned to Al in Al oxide. Therefore, as derived from XPS results, the main species on the pristine sample are Mg, $Mg(OH)_2$, Al and Al_2O_3.

3.2.2. Results for corroded samples

After 15 min immersion in the NaCl solution extra peaks due to traces of Cl^- and Zn^{++} can be observed in the XPS core-level spectra at the energy regions around 199.3 eV for Cl2p, 1022.3 and 1046.3 eV for $Zn2p_{3/2,1/2}$, respectively. In addition, it is found that the peaks in the O1s, Mg2p and Al2p core-level spectra become broadened. As shown in Fig. 5b the O1s peak at 533.6 eV increases its intensity relative to that of the peak at 531.2 eV. Careful peak synthesis of the O1s spectrum results in the appearance of a third component peak at 532.5 eV, which may be attributed to the oxide species in the corrosion layer. Similarly the intensities of Mg2p peak at 51.8 eV (Fig. 6b) and Al2p peak at 74.6 eV (Fig. 7b) are enhanced relative to those at lower binding energies, indicating that oxides of Mg and Al may have resulted from the corrosion.

The advance of corrosion becomes more evident in the sample immersed for 20 min. As shown in Fig. 5c, further increase in the intensity at 532.8 eV, which is assigned to the oxide species, is observed in the O1s spectrum, while in the Mg2p and Al2p spectra, significant peaks at 51.2 and 74.6 eV arise, even stronger than their low energy components, indicating that the sample surface after 20 min immersion is mainly covered by Mg and Al oxides.

Figs 5d, 6d and 7d show additional peaks arising at lower binding energy in the O1s, Mg2p and Al2p regions, i.e. at 530 eV for O1s, at 48.6 eV for Mg2p and 72.0 eV for Al2p, respectively, for the sample immersed for 30 min. After longer immersion, for 60 min, Mg hydroxide becomes the predominant surface species over oxides (Figs 6e and 7e). Nevertheless, species with lower binding energy (Figs 6d and 7d for the sample immersed for 30 min) remain on the surface. For the samples immersed for longer than 15 min chloride ions can still be detected by detailed scans, but neither Nd nor Zn is observed by XPS.

The peaks at lower binding energy in Figs 5d, 6d and 7d may be attributed to differential charging. As previously described by Barr [16–18], the oxide overlayers may show different amounts of charging shift from their metallic substrate upon photoionization. The metallic substrate beneath the surface appears to have smaller charging shifts as compared with

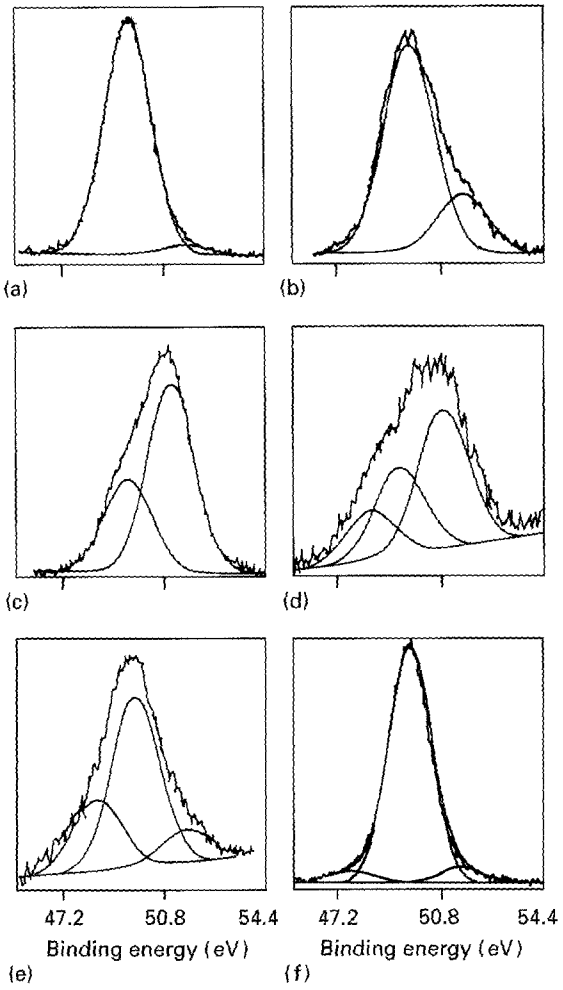

Figure 6 XPS Mg2p core-level spectra corresponding to Fig. 5a–f.

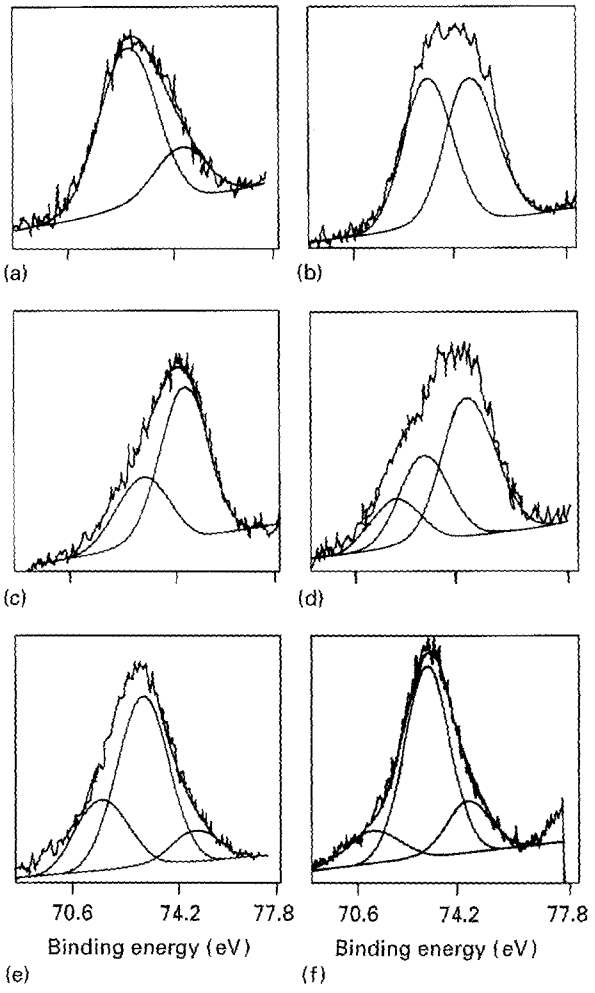

Figure 7 XPS Al2p core-level spectra corresponding to Fig. 5a–f.

those oxide overlayers. If the same amount of energy is applied to correct for different charging shifts, negative chemical shifts for the metallic substrate may then result. This means that the peaks at 48.6 eV for Mg2p and 72.0 eV for Al2p regions in Figs 6d and 7d are due to metallic Mg and metallic Al, respectively. The angle-resolved XPS results support this view. When the take-off angle (with respect to the sample surface) of photoelectrons is changed from 70 to 20°, the intensities of those peaks at lower binding energy are observed to be greatly reduced as shown in Figs 6f and 7f, indicating that these peaks are mainly contributed from the species beneath the surface, most likely the metallic Mg and Al. This phenomenon has been observed in other rapidly solidified Mg and Al based alloys with oxide overlayers on the samples [19].

The XPS results for the corroded samples indicate that the main species on the surface is $Mg(OH)_2$ together with small amounts of MgO and Al_3O_2. No Nd and Zn were observed by XPS.

3.3. Results of AES

Fig. 8a is the Auger electron spectrum (AES) for the pristine sample, showing that C, O and Mg are the main elements detectable by AES on the surface. Al, Nd and Zn are not detectable on the sample surface. The kinetic energy of the MgKLL peak is found to be 1174 eV; 12 eV lower than that of metallic Mg [15]. The chemical shift measured in AES may indicate that Mg species on the sample surface has been oxidized and is in a high oxidation state. This provides support to the assignment of Mg2p core-level peak to the $Mg(OH)_2$ species in the XPS studies.

After immersion, the carbon signal observable in XPS wide scan spectrum (Fig. 9) is greatly reduced in the AES spectrum, whereas chlorine becomes detectable in addition to the main peaks of Mg and O (Fig. 8b).

3.4. SIMS

Fig. 10 displays the positive secondary ion mass spectrum for the pristine sample, indicating that the main species on the surface are Mg, (whose masses and isotopic abundances are 24 amu, 79%; 25 amu, 10%; and 26 amu, 11%), Mg hydroxide (masses 41, 42 and 43), MgO (mass 40) and Al (mass 27). Nd, NdO, Zn and ZnO are barely detectable by SIMS.

Fig. 11 is the SIMS spectrum for the sample after immersion. The dominant surface species are shown to be Mg, MgOH, Al and H. The intensity of the hydrogen peak is observed to increase with the increase in immersion time in NaCl solution.

The results of SIMS depth profiling are given in Figs 12 and 13 for the pristine surface and the surface of the sample immersed for 10 min. For the pristine sample, the relative intensities of Mg, Al and Zn secondary ions in the surface region remain almost the same as in the bulk, although they are all enhanced

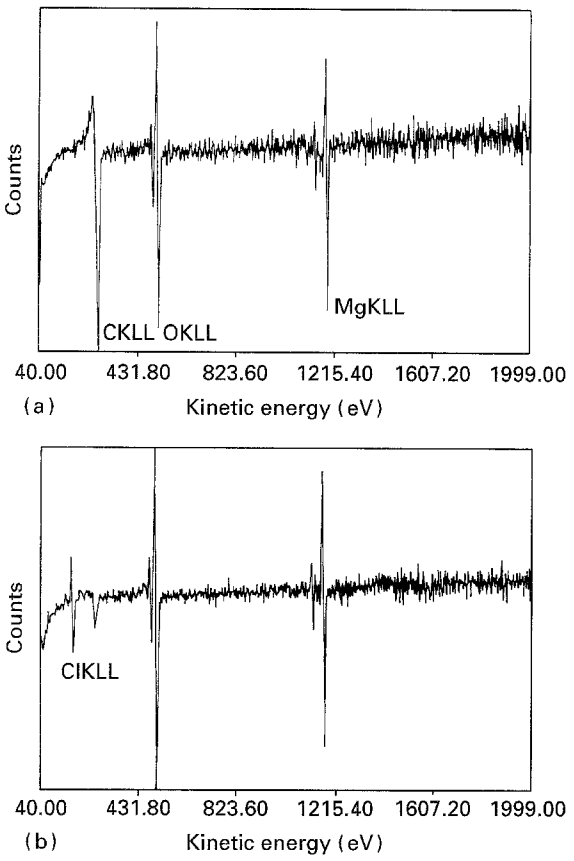

Figure 8 AES spectra of EA55RS (a) as-polished, and (b) after immersion in 3% NaCl solution for 5 min.

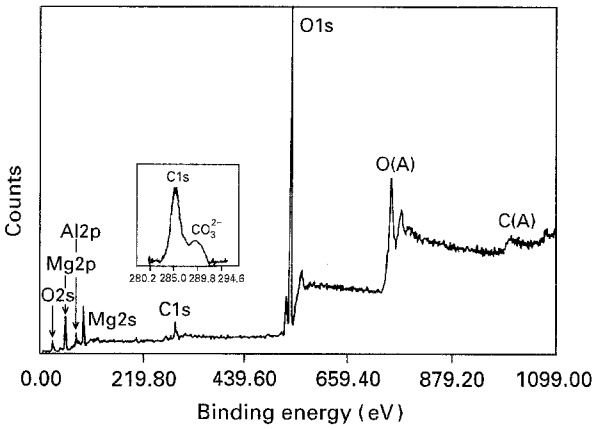

Figure 9 XPS wide-scan spectrum of EA55RS after immersion in 3% NaCl solution for 60 min. The C1s survey scan spectrum is also included.

probably as a result of the presence of oxygen on the surface. The intensities of the secondary ions of oxygen and hydroxide group are low and observed mainly in the surface region only. For the immersed sample, the intensities of the oxygen and hydroxide secondary ions increase (Fig. 11b). In particular, the presence of OH in the bulk, which is not detected for the pristine sample, becomes observable in the corroded area, and even more abundant than MgO species. The surface enhancement of Mg and Al is no longer observed. Rather, the depletion of all metals, in particular, Al and Nd, in the surface region becomes obvious. It is noted that no carbonate species are shown in the SIMS spectra.

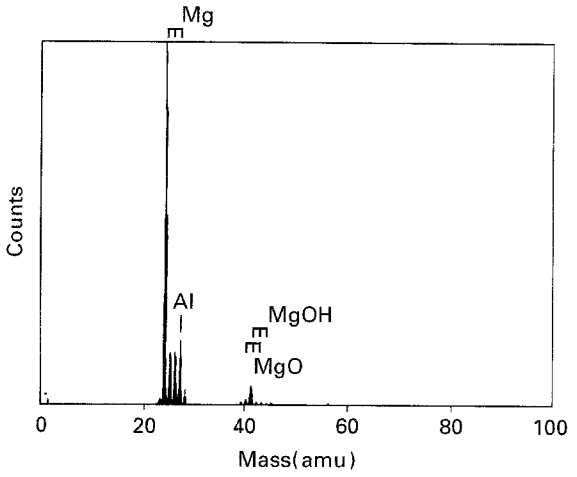

Figure 10 Positive SIMS for pristine EA55RS sample.

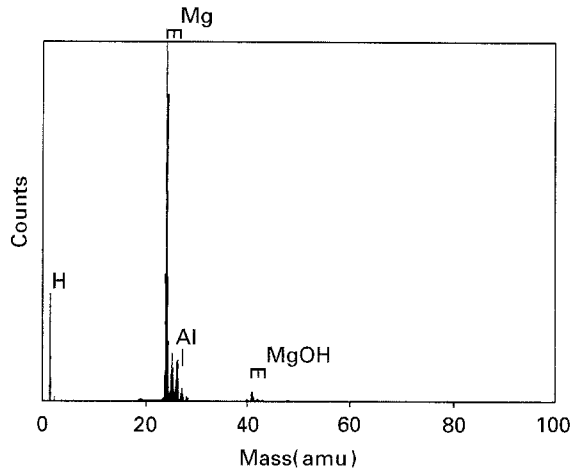

Figure 11 Positive SIMS for EA55RS sample after immersion for 15 min in 3% NaCl solution.

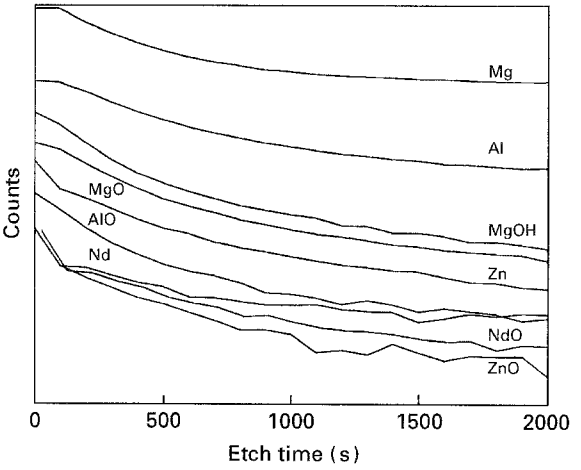

Figure 12 Results for SIMS depth profiling of pristine EA55RS sample.

4. Discussion

The surface characterization of splat quenched Mg–Al binary alloys (with Al content up to 16 wt %) after immersion in 3% NaCl solution have been carried out extensively using XPS, Rutherford Backscattering Spectrometry (RBS), XRD, SEM and transmission electron microscopy (TEM) [3–7]. $Mg(OH)_2$ and

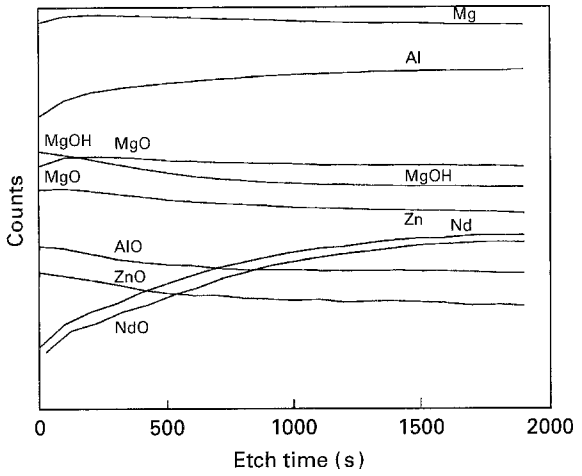

Figure 13 Results for SIMS depth profiling of EA55RS after immersion for 20 min in 3% NaCl solution.

MgO were found on the as-quenched samples. $Mg(OH)_2$ and hydromagnesite ($3MgCO_3 \cdot Mg(OH)_2 \cdot 3H_2O$) were found on the corroded Mg–3.5 Al wt % splat, while Mg spinel ($MgAl_2O_4$) was found along with $Mg(OH)_2$ and MgO for the corroded samples with Al content higher than 10 wt %. The formation of hydromagnesite was found to depend on the storage and handling procedures used. The present XPS and XRD results confirm the presence of $Mg(OH)_2$ on the pristine and corroded surfaces of the samples. Despite the fact that the Al content in the sample is 5 wt %, XRD analysis shows no presence of spinel ($MgAl_2O_4$) and hydromagnesite [$3MgCO_3 \cdot Mg(OH)_2 \cdot 3H_2O$]. On the basis of the XPS results it appears that MgO seems to be less stable than $Mg(OH)_2$ and MgO formed in the early stages of corrosion, while $Mg(OH)_2$ becomes dominant after longer time immersion (60 min, Fig. 6e). The SIMS depth profiling results also indicate that for the corroded sample (Fig. 13) $Mg(OH)_2$ is predominant on the surface, and decreases with depth; while MgO exhibits the opposite trend. This is consistent with a previous finding for rapidly solidified Mg–Al alloys [3].

The effect of the addition of rare earth elements on the corrosion resistance of rapidly solidified Mg based alloys has been subjected to investigation recently by many people [1, 9, 11, 19–21]. Das and Chang [1] reported that Nd containing EA55RS gave a dissolution rate in 3% NaCl of 11 mil yr^{-1} compared with 50 mil yr^{-1} for Nd-free AZ91 HP-T6. Ahmed *et al.* [9] confirmed that Nd could improve the corrosion resistance of Mg alloys under certain circumstances. Rugg *et al.* [20] reported introduction of 1 wt % Nd as a ternary addition gives further reduction in dissolution rate in 3% NaCl for splat quenched Mg–4.7 wt % Mn alloy after 50 h immersion. The improvement in corrosion resistance by the addition of rare earths, such as Nd, to Mg alloys was attributed [2, 20] to a combination of formation of a protective or semi-protective film on the surface of the sample as a result of a reaction of the saline solution with the rare earth, of the reduced pitting corrosion resulting from inertness of second phase particles and of the refined microstructure obtained through rapid solidification. Krishnamurthy *et al.* [21] reported that in rapidly solidified Mg–20 wt % Nd alloy the onset of pseudopassivation was accompanied by an enrichment of the surface in Nd. The present XPS and AES results, however, show that no Nd is detected in the surface region, i.e. within 10 nm of the surface, for either pristine or corroded samples. The SIMS results (for the depth of 0.4 to 2 μm) clearly show that there is a depletion of Nd on the surface of the corroded sample. Although Nd is detected by EDX, the signal is from both oxidation layer and the bulk, since the depth resolution of EDX is ~0.5 μm, more than the thickness of the oxidation layer on the sample. The depletion of rare earth elements in Mg alloys after corrosion was also found in other Mg based rare earth containing alloys [19]. Whether the depletion of rare earth elements has any effect on the formation of these protective films remains unknown.

5. Conclusions

Extrusions of rapidly solidified EA55RS were immersed in 3% NaCl solution for up to 24 h. EDX analyses of the pristine and corroded samples showed that the oxygen content increased as the immersion time increased. $Mg(OH)_2$ and MgO were found on the pristine and corroded surfaces of EA55RS samples by XPS; however, $Mg(OH)_2$ was found to be the dominant species on the surface by SIMS. The content of MgO increased as the depth increased on the surface. There was a depletion of Nd and Zn on the corroded sample surfaces.

Acknowledgements

The authors are grateful to Magnesium Electron Ltd and British Aerospace (UK) for supplying the EA55RS samples. YL is grateful for a grant from the National University of Singapore for the research on the rapid solidification of light metals.

References

1. S. K. DAS and C. F. CHANG, US Patent, 4765954, August (1988).
2. *Idem, ibid.* August 4853035 (1989).
3. C. B. BALIGA, P. TSAKIROPOULOS and J. F. WATTS, *Internal. J. Rapid Solidification* **4** (1989) 231.
4. C. B. BALIGA, P. TSAKIROPOULOS and C. JEYNES, *J. Mater. Sci.* **26** (1991) 1497.
5. C. B. BALIGA and P. TSAKIROPOULOS, *Mater. Sci. Eng A* **A134** (1991) 1029.
6. *Idem, Mater. Sci. Technol.* **9** (1993) 507.
7. *Idem, ibid.* **9** (1993) 513.
8. J. D. COTTON and H. JONES, *Internal. J. Rapid. Solidification* **4** (1991) 55.
9. D. S. AHMED, R. G. J. EDYVEAN, C. M. SELLARS and H. JONES, *Mater. Sci. Technol.* **9** (1990) 469.
10. G. L. MAKER and J. KRUGER, *J. Electrochem. Soc.* **137** (1990) 414.
11. G. L. MAKER, J. KRUGER and K. SIERADZKI, *ibid.* **139** (1992) 47.
12. R. E. LEWIS, A. JOSHI and H. JONES, in "Processings of Structural Metals by Rapid Solidification" edited by F. H. Froes and S. J. Savage (ASM International, Metals Park, OH, 1987) p. 367.

13. R. K. H. KALIMULLIN and A. T. BERDNIKOV, *Zashch Met.* **22**(2) (1986) 262.
14. F. HAHMANN, F. SOMMER, H. JONES and R. G. J. EDYREAN, *J. Mater. Sci.* **24** (1989) 2369.
15. J. CHASTAIN (editor) "Handbook of X-ray Photoelectron Spectroscopy" (Perkin–Elmer, Eden Prairie, M, 1990).
16. T. L. BARR, *J. Vac. Sci. Technol.* **A7**(3) (1989) 1677.
17. *Idem, Surf. Interface Anal.* **4** (1982) 185.
18. *Idem, Appl. Surf. Sci.* **15** (1983) 1.
19. J. LIN, Y. LI, F. C. LOH and K. L. TAN, Unpublished work.
20. D. RUGG, R. G. J. EDYVEAN and H. JONES, *Mater. Sci. Technol.* **9** (1993) 994.
21. S. KRISHNAMURTHY, M. KHOBAIB, E. ROBERTSON and F. H. FROES, *Mater. Sci. Eng.* **99** (1988) 507.

Received 28 June
and accepted 21 December 1995